I&EC research
Industrial & Engineering Chemistry Research

pubs.acs.org/IECR
Article

Self-Similar Pressure-Atomized Sprays with Heat and Mass Transfer

H. Steiner, H. Hinterbichler, and G. Brenn*

Cite This: *Ind. Eng. Chem. Res.* 2023, 62, 17041−17051
Read Online
ACCESS | Metrics & More | Article Recommendations

ABSTRACT: In pressure-atomized sprays, the liquid droplets and the gas in the two-phase flow field may exhibit self-similar properties, so that the spray flow as a whole may be described as self-similar. This description is used to model the mass transfer from the droplets to the ambient gas by evaporation of the droplet liquid. The concentration of the vapor phase is described as the solution of the related transport equation in a self-similar form. The self-similar transform of the mass source of vapor representing the effect of droplet evaporation is compared against profiles obtained from the Frössling correlation for the Sherwood number as a function of the Schmidt and Reynolds numbers. The vapor concentration at the droplet surface depends on the droplet temperature, which converges to the wet-bulb temperature determined by the local vapor content of the ambient air and the dry-bulb air temperature. The self-similar structure of the vapor concentration field and the respective vapor source are determined.

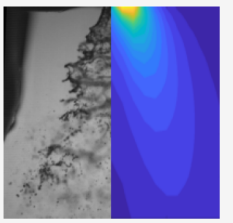

INTRODUCTION

Technical sprays are produced by the atomization of a liquid in an ambient gaseous medium. Applications like spray combustion, spray drying and coating, agricultural crop spraying, and medical sprays have been, and still are, extensively studied.[1,2] Recent developments in nanotechnology enable the utilization of engineered nanoparticles in consumer spray products, like waterproofing sprays, and body-care products, such as hair sprays and deodorants, to enhance the desired effects.[3] Free jet flows, potentially also with two-phase fluid media, such as sprays, are candidates for self-similar dynamic behavior. The subject of the present study is a self-similar description of evaporating pressure-atomized sprays.

Self-similarity is a phenomenon, which is well-known for flows and transport processes without imprinted length or time scales.[4] An example is the self-similar solution for the flow field of a single-phase submerged round jet by Schlichting,[5] which was confirmed by experiments.[6,7] In pressure atomization by the ejection of a liquid into a gaseous environment, a flow field is induced in the otherwise quiescent gas phase. Self-similar behavior of such sprays is also known from the literature. Wu et al.[8] investigated diesel-type sprays and reported self-similar axial velocity profiles far downstream from the nozzle exit, where the droplets and the gas phase are assumed to be in dynamic equilibrium. Recently it has been shown that the progression of this type of spray flow toward an equilibrium state also exhibits self-similarity.[9] The self-similar analysis provided an analytical description of the gas flow field and of the rate of momentum transfer from the liquid to the gas phase. Soltani et al.[10] found self-similar regions of normalized mean droplet velocities and normalized Sauter-mean diameters in sprays from liquid−liquid coaxial swirl atomizers. Based on self-similar assumptions for several characteristics of the flow field, Cossali[11] developed a one-dimensional model to predict the rate of gas entrainment into nonevaporating full-cone sprays. A recent experimental study by Dhivyaraja et al.[12] showed dynamic similarity of the mean droplet velocities, the Sauter-mean diameters, the liquid volume fluxes, and the probability density functions (PDFs) of the droplet diameter in a certain cross section, 19 nozzle diameters downstream from the nozzle orifice, between sprays generated by pressure-swirl atomizers in a wide range of different flow conditions. For the theoretical description, the authors used the similarity coordinate of the single-phase jet[5] and modified it by introducing a constant geometrical parameter of the spray. Sprays from a pressure atomizer with off-axis liquid supply to the nozzle, as relevant for use with consumer-type spray cans, were studied in by Hinterbichler et al. for the self-similarity of both the gas and the droplet flow fields.[9] Three sprays of two different liquids under different flow conditions were examined. The liquid mass flow rates in the sprays corresponded to the order of magnitude of many consumer sprays. The three sprays investigated exhibited two different values of the Weber number of the liquid flow through the nozzle orifice, We_l, and of the liquid Ohnesorge number Oh_l. The size and two velocity components of 10^5 droplets at each point of measurement in the spray flows were measured by phase-Doppler anemometry (PDA) in cross sections at different distances from the atomizer orifice. This method provided a high statistical reliability of the droplet data, even at the edges of the droplet size and velocity spectra. In the

Special Issue: MTCUE-2022

Received: May 8, 2023
Revised: June 21, 2023
Accepted: June 21, 2023
Published: July 7, 2023

https://doi.org/10.1021/acs.iecr.3c01545
Ind. Eng. Chem. Res. 2023, 62, 17041−17051

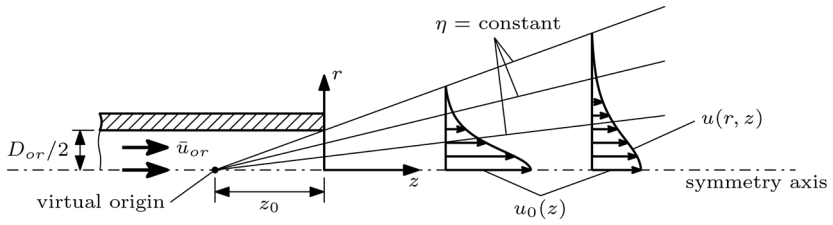

Figure 1. Flow field of an axisymmetric single-phase submerged jet. Reproduced with permission from Hinterbichler et al.[9] Copyright 2020 Cambridge University Press.

regions of the sprays investigated, the flow field exhibited a momentum transfer from the liquid to the gas phase.

There is also evidence of self-similarity in sprays produced by twin-fluid atomization. In air-assisted atomization, Li and Shen,[13] as well as Aryapadi et al.,[14] showed self-similar mean axial droplet velocity profiles. Other authors modeled the spray as a self-similar single-phase jet with variable density, resulting in similar scaling variables as obtained for the single-phase case.[15] In many of the studies discussed above, liquid and gas were injected simultaneously, resulting in negligible slip between the two phases. Thus, the cross-sectional averages of liquid and gas momentum flow rates remain approximately constant, endorsing self-similarity as observed for the single-phase jet.[16]

In some literature, the self-similarity of evaporating sprays is addressed. In spray flames, Karpetis and Gomez[17] showed self-similarity of the evaporation source term. Russo and Gomez[18] showed self-similar axial velocity profiles in buoyancy-dominated laminar spray flames. Kourmatzis et al.[19] reported self-similar axial velocity profiles for the two different droplet size classes, $d < 10\ \mu$m and $40\ \mu\text{m} < d < 50\ \mu$m, in nonreacting sprays and turbulent spray flames in the vicinity of the nozzle exit (approximately one to ten nozzle diameters downstream from the orifice). Additionally, they indicate self-similar turbulence intensities deduced from the motion of the smallest droplets ($d < 10\ \mu$m). Shearer et al.[20] and Faeth[21] modeled evaporating sprays in spray combustion as free submerged jets with variable fluid density. Petranović et al.[22] developed a numerical method for simulating evaporating unsteady spray flows with relevance for fuel injection in internal combustion engines. The simulations yielded the time-dependent spray geometry, the spray penetration length as a function of time, and the radial profiles of the mixture fraction at different distances from the injector exit.

In the present work, we focus on the flow fields of sprays from single-fluid pressure atomization, where the motion of the gas phase is induced by momentum transfer from the liquid phase exclusively. Thus, the rate of liquid momentum transport through every spray cross section decreases with an increasing distance from the atomizer orifice, while the gas phase gains momentum. The study extends the self-similar description of the spray flow developed by Hinterbichler et al.,[9] valid in the region dominated by momentum transfer from the droplets to the gas phase, deriving a self-similar description of evaporating pressure-atomized sprays. The concept of self-similarity has been established as a useful approach for solving partial differential equations analytically. Its principal benefits and limitations are discussed in much detail in the seminal review by Barenblatt and Zel'dovich.[23] Self-similar descriptions of flow fields are attractive because they reveal deep insight into the transport processes governing the flow, they allow for a universal description even of complex flow, they determine important scaling laws, e.g., for mass and momentum, and they are computationally efficient.

In the following section, the derivation of the self-similar description of the two-phase flow fields of the sprays is revisited. Then, the self-similar representation of the transport equation for the concentration of a gaseous mixture component is derived. In this, the self-similar modeling of the vapor source due to the droplet evaporation plays a key role. The modeling results are discussed in view of the global spray behavior. The paper ends with the conclusions.

SELF-SIMILAR MOMENTUM TRANSPORT

Self-similar momentum transport in pressure-atomized spray flow, in the region of the sprays where momentum is transferred from the liquid to the gas phase, i.e., with large slip velocities between the droplets and the gas, was reported.[9] The self-similar description of the gas flow field in the spray flow, accounting for momentum transfer between the phases, is revisited in the present section and extended to account for self-similar mass transfer in the next section.

The flow field of the gas phase in the spray is sketched in Figure 1. The mathematical description of the gas flow is based on a boundary-layer approximation with a negligible azimuthal velocity component and constant pressure throughout. The contribution of the viscous shear stress is neglected against the turbulent contribution, which is modeled using the Boussinesq eddy viscosity concept. Accordingly, the two-dimensional axisymmetric boundary-layer equations read

$$\frac{\partial u_z}{\partial z} + \frac{1}{r}\frac{\partial (r u_r)}{\partial r} = 0 \tag{1}$$

$$u_z\frac{\partial u_z}{\partial z} + u_r\frac{\partial u_z}{\partial r} = \nu_t \frac{1}{r}\frac{\partial}{\partial r}\left(r\frac{\partial u_z}{\partial r}\right) + f_{d,z} \tag{2}$$

The gas velocity components in the axial and radial directions are denoted by u_z and u_r, respectively. ν_t is the turbulent eddy viscosity, assumed to be constant, and $f_{d,z}$ represents the momentum source due to momentum transfer from the liquid droplets to the gas, which couples the axial gas momentum balance (eq 2) to the axial momentum balance of the liquid phase.[9] The latter is given by

$$\frac{\partial}{\partial z}\left(\rho_l \sum_{j=1}^{J} \bar{u}_{l,j}\phi_{z,j}\right) + \frac{1}{r}\frac{\partial}{\partial r}\left(r\rho_l \sum_{j=1}^{J} \bar{u}_{l,j}\phi_{r,j}\right) = -\rho f_{d,z} \tag{3}$$

where the subscript j denotes a droplet size class, $\bar{u}_l$ the axial number-mean droplet velocity and ϕ the droplet volume flux. The ansatz for the self-similar solution for the gas phase reads

$$\eta = D\frac{r}{(z - z_0)^{\alpha}} \tag{4}$$

https://doi.org/10.1021/acs.iecr.3c01545
Ind. Eng. Chem. Res. 2023, 62, 17041−17051

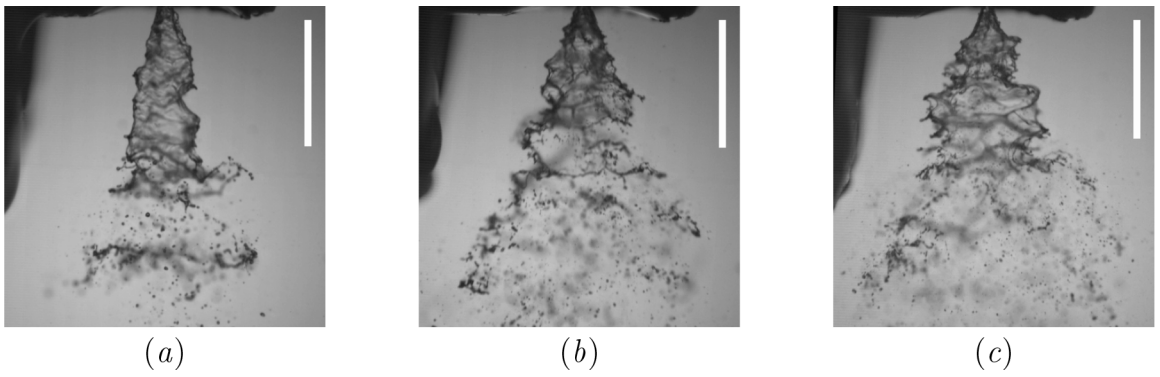

Figure 2. Instantaneous photographs of (a) spray 1, (b) spray 2, and (c) spray 3. The images were acquired with a high-speed camera at a frame rate of 10 000 frames per second, with an exposure time of 307 000^{-1} s per frame. The white bar corresponds to a length of 5 mm. Reproduced with permission from Hinterbichler et al.[9] Copyright 2020 Cambridge University Press.

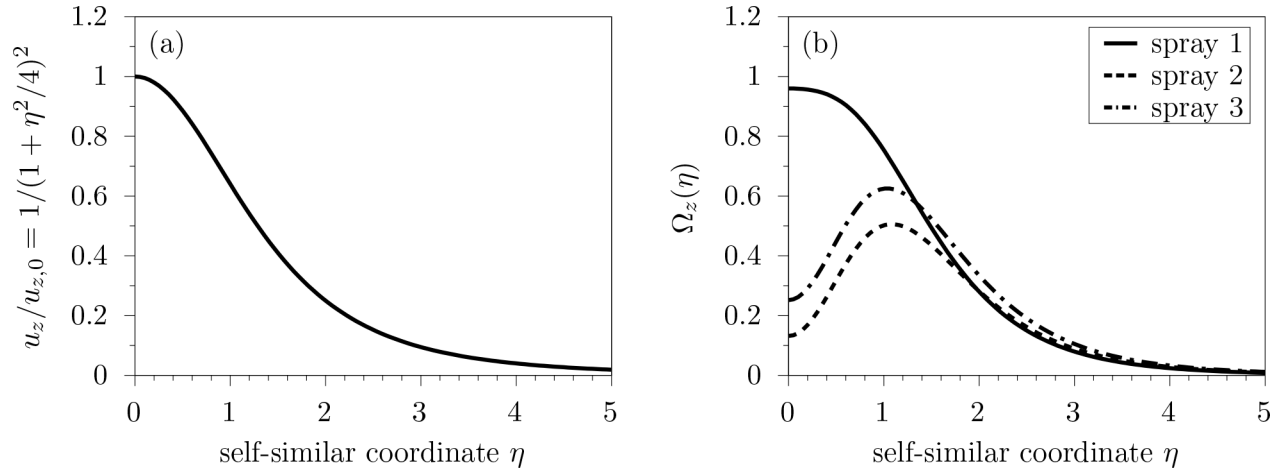

Figure 3. (a) Universal self-similar axial gas velocity profile (eq 15). (b) Self-similar shape functions of the momentum source term (eq 13) in the three sprays. The parameters of the self-similar description are listed in Table 1.

$$\Psi = C(z - z_0) f(\eta) \tag{5}$$

$$f_{d,z} = C^2 D^4 (z - z_0)^{1-4\alpha}\, \Omega_z(\eta) \tag{6}$$

Here, η represents the self-similar coordinate and Ψ the Stokesian stream function. $f(\eta)$ and $\Omega_z(\eta)$ denote the self-similar shape functions of the gas flow field and the momentum source, respectively. z_0 is the virtual origin of the flow field. The exponent α determines the curvature of lines η = constant in the (r, z) space. The constants C and D are required for dimensional reasons and for scaling.

Figure 2 shows instantaneous photographs of the three sprays. Sprays resulting from a pressure atomization process are characterized by the values of the Weber and Ohnesorge numbers, defined as

$$We_l = \rho_l D_{or} u_{or}^2/\sigma \tag{7}$$

$$Oh_l = \mu_l/(\rho_l \sigma D_{or})^{1/2} \tag{8}$$

In these definitions, D_{or} denotes the diameter of the atomizer orifice, u_{or} denotes the mass-flow mean liquid velocity through the atomizer orifice, ρ_l denotes the liquid density, μ_l denotes the liquid dynamic viscosity, and σ denotes the liquid surface tension against air.

The axial and radial velocity components calculated from the Stokesian stream function as per

$$u_z = \frac{1}{r}\frac{\partial \Psi}{\partial r} = CD^2 (z - z_0)^{1-2\alpha} \frac{f'}{\eta} \tag{9}$$

$$u_r = -\frac{1}{r}\frac{\partial \Psi}{\partial z} = CD(z - z_0)^{-\alpha}\left(\alpha f' - \frac{f}{\eta}\right) \tag{10}$$

satisfy the continuity eq 1. Accordingly, we transform the z-momentum equation of the gas phase (eq 2) into the self-similar representation

$$(1 - 2\alpha) f'^2 - \eta f\left(\frac{f'}{\eta}\right)' = \frac{\nu_t}{C}\eta\left[\eta\left(\frac{f'}{\eta}\right)'\right]' + \eta^2 \Omega_z \tag{11}$$

Assuming the self-similar profile of the stream function as

$$f(\eta) = \frac{\eta^2}{1 + \eta^2/4} \tag{12}$$

the self-similar form (eq 11) of the z-momentum balance allows the self-similar shape function of the momentum source to be determined as

$$\Omega_z(\eta) = \frac{2}{(1 + \eta^2/4)^4}\left[2(1 - 2\alpha) + \eta^2 + \frac{\nu_t}{C}(2 - \eta^2)\right] \tag{13}$$

https://doi.org/10.1021/acs.iecr.3c01545
Ind. Eng. Chem. Res. 2023, 62, 17041−17051

Figure 3(a) depicts the self-similar shape function of the axial gas velocity u_z, which was normalized with its value at the spray axis, i.e., at $\eta = 0$:

$$u_{z,0} = CD^2(z - z_0)^{1-2\alpha} f''(0) \tag{14}$$

using eqs 9 and 12 to yield

$$\frac{u_z}{u_{z,0}} = \frac{f'(\eta)}{\eta f''(0)} = \frac{1}{(1 + \eta^2/4)^2} \tag{15}$$

It is bell-shaped, with the maximum at the symmetry axis, and universal in the sprays investigated. The self-similar shape functions of momentum source $\Omega_z(\eta)$ are shown in Figure 3(b). They differ between the three sprays. In spray 1, a bell-shaped curve with a maximum at the spray axis can be observed. In sprays 2 and 3, the profiles exhibit a local minimum at the spray axis and a local off-axis maximum. The shapes of the profiles reflect the different regimes of atomization. In spray 1, at a lower Weber number, the conical sheet emerging from the orifice is not fully open, which corresponds to the so-called tulip-stage atomization regime. In the two other sprays, the sheet is open, which leads to finer atomization and a larger concentration of liquid mass and momentum at the location of the liquid sheet. This is indicated by the off-axis maxima of the profiles shown in Figure 3(b).

The gas-phase momentum flow rate through every cross section z = constant increases with the axial distance from the atomizer due to the momentum source in eq 2. Its axial scaling can by derived with the self-similar description of the gas flow field from the general definition of the axial gas momentum flow rate

$$\begin{aligned} \mathcal{I}(z) &= 2\pi\rho \int_{r=0}^{\infty} u_z^2 r \, \mathrm{d}r \\ &= 2\pi\rho C^2 D^2 (z - z_0)^{2-2\alpha} \int_{\eta=0}^{\infty} \frac{f'^2}{\eta} \, \mathrm{d}\eta \\ &= \frac{16}{3}\pi\rho C^2 D^2 (z - z_0)^{2-2\alpha} \end{aligned} \tag{16}$$

Here, ρ represents the gas density. Using the velocity data measured by PDA, the values of the parameters z_0, α, C, and D are determined by a best fit of the experimentally measured axial variation of the centerline velocity $u_{z,0}(z)$ and the momentum flow rate $\mathcal{I}(z)$ to the z-dependencies in eqs 14 and 16, respectively, and by enforcing the experimentally measured normalized velocities $u_z/u_{z,0}$ = const. along $\eta = D\, r/(z - z_0)^{\alpha}$ = const. to comply with the self-similarity of the profiles of $u_z/u_{z,0}$. The values of the model parameters reported by Hinterbichler et al.[9] are listed in Table 1, together with the liquid flow conditions of the three sprays investigated. The exponent $\alpha \approx 2/3$ for all of the cases. The spray flows are characterized by the liquid Weber and Ohnesorge numbers. For sprays 1 and 2, demineralized water was used as the test liquid. Spray 3 used a mixture of ethanol and demineralized water with 10 mass percent of ethanol, thus modifying the liquid viscosity to allow for a different Ohnesorge number, while keeping the Weber number constant.

With the values of $\alpha < 1$ listed in Table 1, the global gas momentum flow rate increases with z. Its axial evolution in the three sprays is depicted in Figure 4(a). Similar to the global gas momentum flow rate, the gas mass flow rate, $\dot{m}$, can be derived from a self-similar description. It is defined as

Table 1. Model Parameters Reported in Hinterbichler et al.[9]

	spray 1	spray 2	spray 3
$\dot{m}_l$ (g/s)	2.00	2.92	2.45
We_l	1395	2974	2921
Oh_l	0.0059	0.0059	0.0099
α	0.66	0.71	0.65
z_0 (mm)	−2.2	−14.8	−3.1
C (m^2/s)	0.0033	0.0051	0.0070
D (m$^{\alpha-1}$)	21.9	18.5	17.3
ν_t (mm^2/s)	120ν[a]	150ν	165ν

[a] ν = 15.4 mm^2/s denotes the kinematic viscosity of air at 20 °C. The nozzle diameter D_{or} was 0.4 mm.

$$\begin{aligned} \dot{m} &= 2\pi\rho \int_{r=0}^{\infty} u_z r \, \mathrm{d}r = 2\pi\rho C(z - z_0) \int_{\eta=0}^{\infty} f' \, \mathrm{d}\eta \\ &= 8\pi\rho C(z - z_0) \end{aligned} \tag{17}$$

It is interesting to note that the exponent α does not appear in eq 17. This implies that the axial dependency of the mass flow rate, $\dot{m} \propto (z - z_0)$, does not change with the value in the exponent of the axial dependency of the gas momentum flow rate, $\mathcal{I} \propto (z - z_0)^{2-2\alpha}$, for all types of flow described by eq 11. This observation is independent of the mathematical solution for the self-similar shape functions $f(\eta)$ and $\Omega_z(\eta)$. The axial evolution of the gas mass flow rate (eq 17) is depicted in Figure 4(b) for the three sprays.

MASS TRANSPORT

For evaporating sprays, the transport equations governing the flow field are extended by including the equation for the transport of the evaporating species mass in the gas phase. The self-similar form of this transport equation is again derived from the boundary-layer theory. A source term accounts for the transfer of the evaporating species into the gas flow field. In the modeling of the rate of mass transfer, the spray droplet temperature is treated as variable, accounting for heat transfer between the spray droplets and the ambient gaseous medium and the related cooling effect for the droplets. The thermal energy balance for the ambient gas is omitted, however, treating its temperature as constant.

Self-Similar Mass Transport Equation. The analysis of self-similar spray flow with account for momentum transfer from the droplet to the gas phase, as reported in ref 9 and revisited in the previous section, is presently extended to describe mass transport of the evaporating species in the gas phase of an evaporating spray. Based on the boundary-layer approximation, the transport of the vapor component mass concentration ρ_i at steady state is described in axisymmetric cylindrical form as

$$u_z \frac{\partial \rho_i}{\partial z} + u_r \frac{\partial \rho_i}{\partial r} = \mathcal{D}_t \frac{1}{r} \frac{\partial}{\partial r}\left(r \frac{\partial \rho_i}{\partial r} \right) + S_i \tag{18}$$

The effective turbulent diffusion coefficient $\mathcal{D}_t$ is assumed to have a constant value throughout the flow field. The term S_i denotes the vapor source due to the evaporation of the spray droplets. Assuming the net rate of production of vapor to be small, we base our analysis on the following assumptions: The presence of the vapor component i does not influence the physical properties ρ and ν of the gas flow field and, therefore, does not change the velocity field determined by eqs 1 and 2; the change of the droplet temperature due to the droplet

https://doi.org/10.1021/acs.iecr.3c01545
Ind. Eng. Chem. Res. 2023, 62, 17041−17051

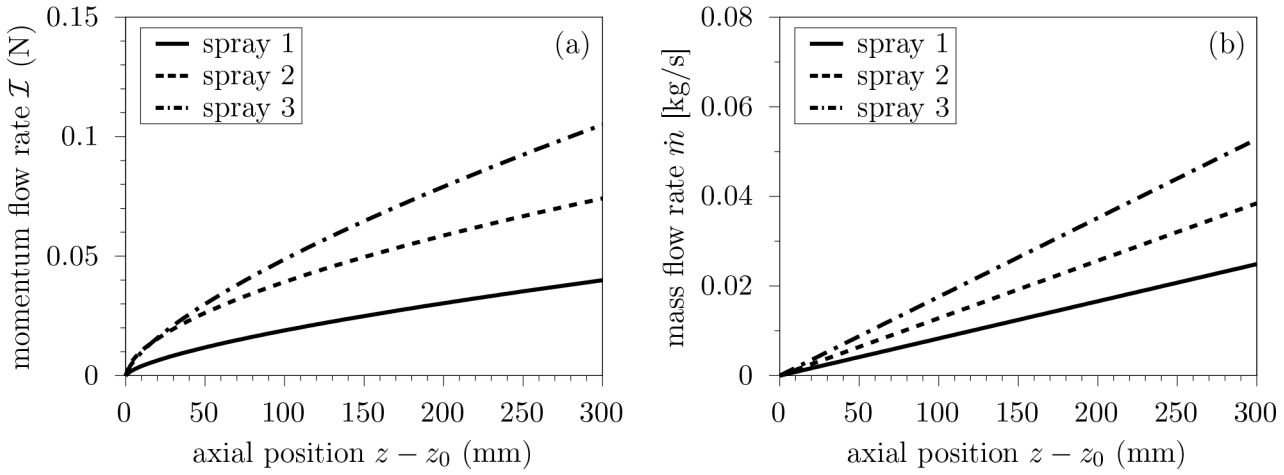

Figure 4. (a) Axial evolution of the gas momentum flow rate according to eq 16. (b) Linear increase of the gas mass flow rate calculated by eq 17. The parameters of the self-similar description for the three sprays are given in Table 1.

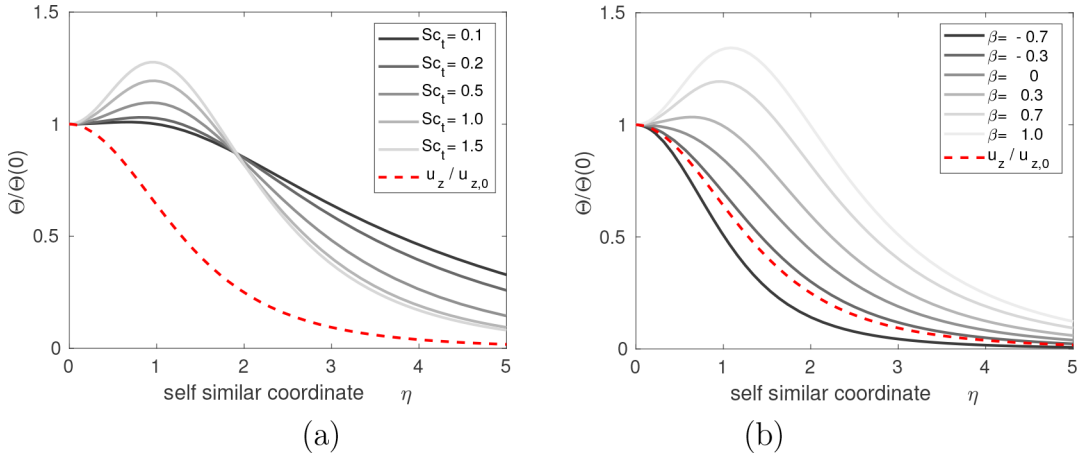

Figure 5. Self-similar vapor concentration profiles obtained from eq 28 for (a) $\beta = 0.7$ and (b) $Sc_t = 1$ in spray 2. To calculate $\Theta(\eta)$, the self-similar shape function of the vapor source $\Phi_i(\eta)$ is set equal to the self-similar shape function of the momentum source (eq 13). The dashed red line represents the self-similar axial gas velocity profile (eq 15).

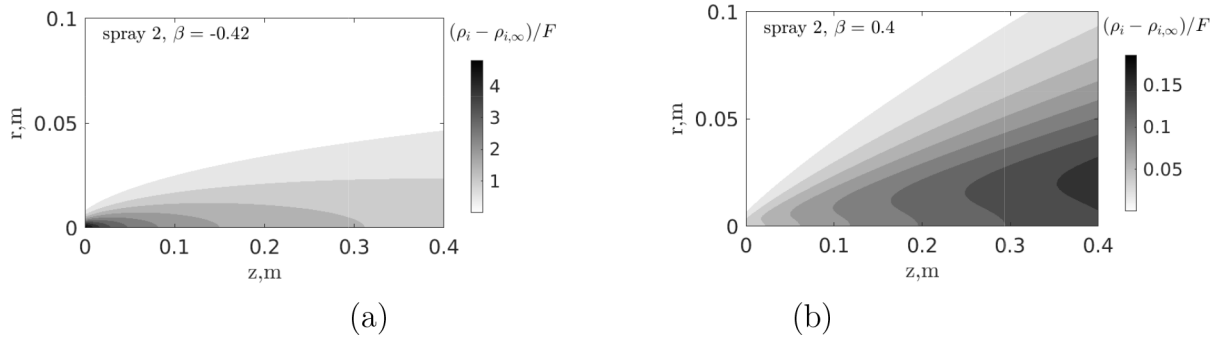

Figure 6. Self-similar normalized vapor concentration fields $(\rho_i - \rho_{i,\infty})/F$ in the meridional r, z plane of spray 2 (a) for $\beta = 1 - 2\alpha = -0.42$ and (b) for $\beta = 0.4$. The evaluation of the field is based on the self-similar shape function of the vapor source $\Phi_i(\eta)$ set equal to the self-similar shape function of the momentum source (eq 13).

evaporation is accounted for, i.e., the cooling of the droplets, making their temperature converge to the wet-bulb temperature, enters the analysis. The value of the wet-bulb temperature is determined by the dry-bulb temperature and the vapor content of the gaseous medium ambient to the droplet. The cooling of the gas phase is not included in the analysis, treating the gas temperature as constant. This assumption requires a sufficiently low rate of spray droplet evaporation, as realized in the present experiments.

For transforming the transport equation 18 into the self-similar form, we introduce the ansatz for the vapor concentration ρ_i reading

$$\rho_i(r, z) - \rho_{i,\infty} = t(z)\,\Theta(\eta) \tag{19}$$

https://doi.org/10.1021/acs.iecr.3c01545
Ind. Eng. Chem. Res. 2023, 62, 17041−17051

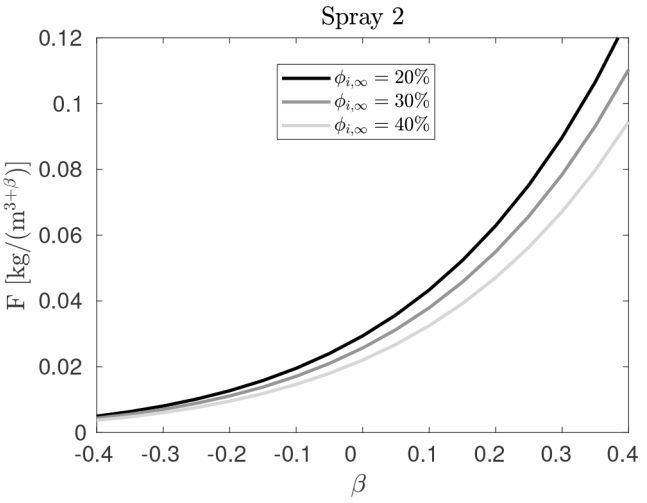

Figure 7. Coefficient F in the self-similar ansatz for the vapor concentration field as a function of the exponent β for spray 2 from ref 9 at varying ambient air relative humidity, with the constant air temperature $T_\infty = 20°$ C.

Table 2. Exponent β and Coefficient F in the Self-Similar Description of the Vapor Concentration in the Spray Flow Field at the Relative Ambient Air Relative Humidity of 30%

	spray 1	spray 2	spray 3
β	0.06	0.09	0.14
F [kg/m$^{3+\beta}$]	0.0151	0.0365	0.0360

where $\rho_{i,\infty}$ is the vapor concentration in the far field ($\eta \to \infty$). The symbol $t(z)$ denotes a scaling function, and $\Theta(\eta)$ represents the self-similar vapor concentration. Introducing eq 19 into eq 18 yields

$$C(z - z_0)\frac{t'}{t} f'\Theta - Cf\Theta' = \mathcal{D}_t(\eta\Theta')' + \frac{(z - z_0)^{2\alpha}}{D^2 t}\eta S_i \tag{20}$$

where the prime denotes the derivative with respect to z for $t(z)$, and with respect to η for $f(\eta)$ and $\Theta(\eta)$. For eq 20 to become an ordinary differential equation, independent of z, we require

$$C(z - z_0)\frac{t'}{t} = \text{constant}: = E \tag{21}$$

resulting in

$$t(z) = F(z - z_0)^{E/C} \tag{22}$$

with the two, yet unknown, constants E and F. Moreover, for self-similarity of the transport eq 20, we require the vapor source term S_i to be of the form

$$S_i(r, z) = \mathcal{D}_t D^2 (z - z_0)^{-2\alpha} t(z)\, \Phi_i(\eta) \tag{23}$$

where $\Phi_i(\eta)$ denotes the yet unknown self-similar shape function of the vapor source. For convenience, we introduce the constant exponent

$$\beta: = \frac{E}{C} \tag{24}$$

Thus, the ansatz for the vapor concentration (eq 19) and the vapor source (eq 23) turn into

$$\rho_i(r, z) - \rho_{i,\infty} = F(z - z_0)^{\beta}\, \Theta(\eta) \tag{25}$$

$$S_i(r, z) = \mathcal{D}_t D^2\, F(z - z_0)^{\beta - 2\alpha}\, \Phi_i(\eta) \tag{26}$$

The constant F is required for dimensional reasons. The exponent β determines the axial scaling of the vapor concentration field and the vapor source. Introducing the turbulent Schmidt number

$$Sc_t = \frac{\nu_t}{\mathcal{D}_t} \tag{27}$$

the self-similar transport eq 20 becomes

$$Sc_t \frac{C}{\nu_t}(\beta f'\Theta - f\Theta') = (\eta\Theta')' + \eta\Phi_i \tag{28}$$

With $\beta = 1$ and $\Phi_i = 0$, eq 28 reduces to the well-known transport equation of the single-phase round jet.[24] The solution of eq 28 is subject to two boundary conditions. We formulate them using the symmetry of the problem and the vapor concentration in the far field

$$\frac{\partial \rho_i}{\partial \eta}|_{\eta \to 0} = 0 \Rightarrow \Theta'(0) = 0 \tag{29}$$

$$\rho_i|_{\eta \to \infty} = \rho_{i,\infty} \Rightarrow \Theta(\eta \to \infty) = 0 \tag{30}$$

Knowledge of the exponent β, the constant F, the turbulent Schmidt number Sc_t, and the self-similar shape function of the vapor source Φ_i is required to determine the self-similar vapor concentration profile $\Theta(\eta)$ from eq 28. For the turbulent Schmidt number, Tominaga and Stathopoulos[25] suggest a value of $Sc_t = 0.9$ in turbulent single-phase free shear flow. The exponent β relates to the global mass flow rate of the vapor component i as per

$$\begin{aligned}\dot{m}_i &= 2\pi \int_{r=0}^{\infty} u_z(\rho_i - \rho_{i,\infty}) r\, \mathrm{d}r \\ &= 2\pi C\, F(z - z_0)^{1+\beta} \int_{\eta=0}^{\infty} f'\Theta\, \mathrm{d}\eta\end{aligned} \tag{31}$$

Since the evaporating spray droplets continuously introduce vapor into the gas phase, it is expected that the vapor mass flow rate $\dot{m}_i$ through the spray cross section increases with the z coordinate in the flow field. For the derivative $\mathrm{d}_i/\mathrm{d}z$ to be positive, we expect that the value of $\beta > -1$. To determine the exact values of the model parameters, data from experiments or simulations on the vapor concentration field in such spray flows is required. Experiments could yield the vapor concentration field in meridional sections in the sprays, e.g., by LIF, with a fluorescent evaporating species, such as acetone. On the other hand, simulations would need to provide the vapor concentration field inside and outside the spray flow field. The data from these results could be the basis for the determination of the self-similar model parameters. With information on the local concentration field $\rho_i(r, z)$, the self-similar behavior may be verified, and the parameters β and F, as well as the self-similar concentration profile $\Theta(\eta)$ may be determined. Furthermore, from eq 28 the shape of the vapor source $\Phi_i(\eta)$ may then be determined and compared to the modeling or simulation data. The PDA measurement data at hand, however, do not allow this. The validation will therefore be the subject of future studies.

Instead, as a parameter study, we determine self-similar concentration profiles from eq 28 for different values of the

https://doi.org/10.1021/acs.iecr.3c01545
Ind. Eng. Chem. Res. 2023, 62, 17041−17051

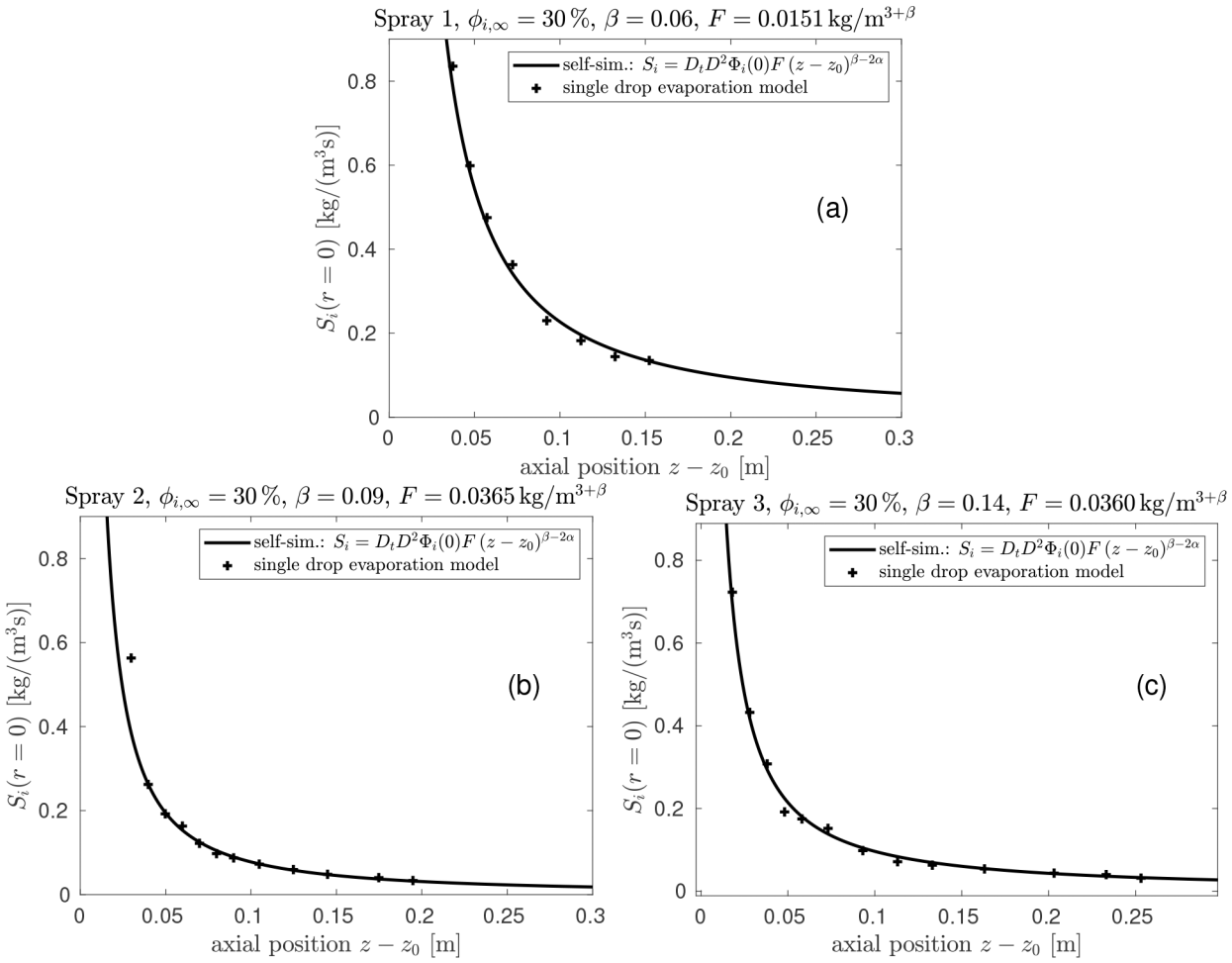

Figure 8. Vapor source S_i according to the self-similar description and from the single-droplet model on the symmetry axes of (a) spray 1, (b) spray 2, and (c) spray 3 at the ambient air relative humidity of 30%.

relevant parameters. For this purpose, we assume the self-similar shape function of the vapor source, $\Phi_i(\eta)$, to be equal to the self-similar shape function of the momentum source (eq 13, i.e., $\Phi_i(\eta) := \Omega_z(\eta)$, hypothesizing that low transfer of momentum from the liquid to the gas phase equivalently translates into low mass transfer due to the droplet evaporation. The low mass transfer rate justifies that, despite the droplet evaporation, the physical properties of the gas phase are treated as constant. In Figure 5, self-similar concentration profiles as solutions of eq 28 are exemplarily depicted (a) for various values of Sc_t, keeping the exponent β constant at the value of 0.7, and (b) for varying β, keeping the turbulent Schmidt number constant at $Sc_t = 1$. For obtaining these profiles, the self-similar parameters of spray 2 were used (Table 1). As expected, a larger Schmidt number results in narrower vapor concentration profiles. In turn, larger values of β reflect a stronger increase in the vapor mass flow rate (eq 31) with increasing z distance from the nozzle orifice, thus resulting in wider self-similar concentration profiles. For total analogy between mass and momentum transfer ($\Phi_i(\eta) = \Omega_z(\eta)$, $\beta = 1 - 2\alpha$, and $Sc_t = 1$), the obtained concentration profile collapses with the self-similar axial gas velocity profile. The latter is depicted by the dashed red lines in Figure 5. Cases with values of Sc_t less than unity exhibit concentration profiles that are flatter than the ones shown.

Evaluating the self-similar concentration profile for specific values of the exponent β, and normalizing the results with the coefficient F, yields the results shown in Figure 6(a),(b) for a negative and a positive value of β in spray 2. The negative value equals $1-2\alpha$ and, therefore, represents a full analogy with the momentum transport. The turbulent Schmidt number $Sc_t = 1$. The self-similar field is turned into a representation in the r, z plane. It is seen that, at a given downstream position, the larger value of β produces a wider radial extension of the vapor field than the smaller one, representing the higher intensity of evaporation in this case. At the higher evaporation rate, the vapor accumulates around the spray symmetry axis with increasing downstream coordinate, since it is not fast enough transported away radially from the spray axis.

Modeling of the Vapor Source. A method is proposed to determine the scaling behavior of the vapor source S_i, which is due to the evaporation of the spray droplets. The source is composed from the contributions by all the spray droplets of different size. A fit of the equation for S_i to the scaling law required for self-similarity will allow values of parameters F and β to be determined.

The contribution to the vapor source from a spray droplet of size d_j, i.e., its evaporation rate, is

$$\dot{m}_{i,j} = \pi d_j^2\, k_j(\rho_{i,s,j} - \rho_i) \tag{32}$$

https://doi.org/10.1021/acs.iecr.3c01545
Ind. Eng. Chem. Res. 2023, 62, 17041−17051

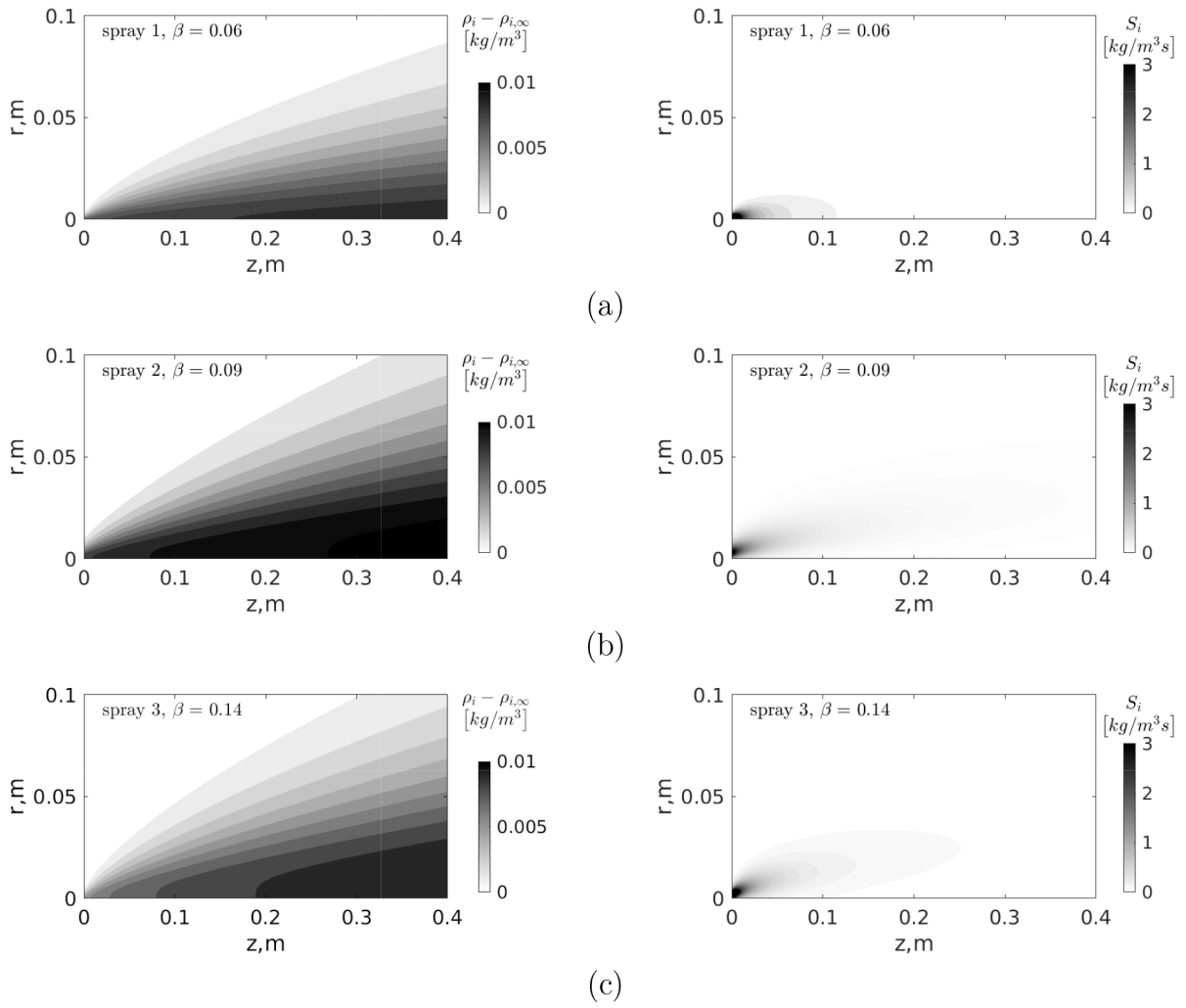

Figure 9. (Left) Vapor concentration field and (right) strength of the vapor source in the flow fields of (a) spray 1, (b) spray 2, and (c) spray 3 at the ambient air relative humidity of 30%.

with the mass transfer coefficient k_j, the vapor concentration $\rho_{i,s,j}$ at the surface of the droplet, and the vapor concentration ρ_i in the air ambient to the droplet, outside the concentration boundary layer. The modeling of S_i therefore requires calculation of the mass transfer coefficient k_j, or its nondimensional equivalent, the Sherwood number Sh_j. For the evaporation of individual spray droplets, the well-known correlation by Frössling[26]

$$Sh_j = \frac{k_j d_j}{\mathcal{D}} = 2 + 0.553\, Re_j^{1/2}\, Sc^{1/3} \tag{33}$$

is suitable. In this correlation, the Reynolds number Re_j of a droplet with size d_j is formed with its velocity relative to the ambient gas phase, as given by

$$Re_j = \frac{d_j|u_j - u_z|}{\nu} \tag{34}$$

The self-similar solution (eq 15) of the z-momentum equation for the gas phase is used for the velocity u_z.[9] Weighting the evaporation rate of individual droplets with the local droplet size-dependent droplet-number concentration, as obtained from the PDA measurement data, yields the following expression for the vapor source

$$S_i = \pi \mathcal{D} \sum_{j=1}^{J} d_j n_j (2 + 0.553 Re_j^{1/2} Sc^{1/3})(\rho_{i,s,j} - \rho_i) \tag{35}$$

Here, d_j denotes the centroid diameter of the jth droplet size class, n_j denotes the corresponding local droplet-number concentration, Re_j denotes the corresponding droplet Reynolds number, and $Sc = \nu/\mathcal{D}$ denotes the molecular Schmidt number. The total number of droplet size classes is J.

Equation 35 is evaluated for locations in the spray flow field along the symmetry axis $r = 0$, i.e., for $\eta = 0$. For doing this, the evolution of the droplet size, the droplet Reynolds number, and the vapor concentration at the droplet surface with the z coordinate is determined. For this purpose, the axial variations of the droplet size d_j, droplet velocity u_j, and droplet temperature T_j are analytically obtained by integrating the balance equations of the droplet mass, momentum and thermal energy, reading

$$\frac{\mathrm{d}d_j}{\mathrm{d}z} = \frac{2\nu}{u_j \rho_l d_j} \frac{Sh}{Sc} (\rho_i - \rho_{i,s,j}) \tag{36}$$

$$\frac{\mathrm{d}u_j}{\mathrm{d}z} = \frac{18\nu\rho}{u_j \rho_l d_j^2} \left(1 + \frac{1}{6} Re_j^{0.8}\right)(u_z - u_j) \tag{37}$$

https://doi.org/10.1021/acs.iecr.3c01545
Ind. Eng. Chem. Res. 2023, 62, 17041−17051

$$\frac{\mathrm{d}T_j}{\mathrm{d}z} = \frac{6\nu}{u_j d_j^2 Sc}\frac{\rho}{\rho_l}\frac{c}{c_l}Sh\left[\frac{h_{lg}}{\rho c}(\rho_i - \rho_{i,s,j}) + Le(T_\infty - T_j)\right] \tag{38}$$

respectively, with respect to the coordinate z along the spray axis. This set of equations follows essentially a concept of Abramzon and Sirignano.[27] The droplet temperature T_j obtained from eq 38 is needed for determining the vapor concentration $\rho_{i,s,j}$ at the droplet surface, i.e., in the saturated state determined by the droplet temperature. This concentration is calculated using the semiempirical correlation[28]

$$\rho_{i,s,j} = \frac{1}{T_j^{8.2}}\exp(77.345 + 0.0057T_j - 7235/T_j)\frac{1}{R_i T_j} \tag{39}$$

which approximates the analytically derived formulation by Hyland and Wexler.[29] With the specific gas constant of the evaporating species R_i in J/(kg K) and the droplet temperature T_j in K, the saturation concentration is obtained in kg/m^3. The self-similar ansatz (eq 25) is substituted for vapor concentration ρ_i. Minimizing the difference between eqs 26 and 35 for the vapor source allows a relation between the parameters β and F to be found for given ambient air relative humidity.

In detail, rewriting the vapor source (eq 35) in the form

$$S_i = \pi\mathcal{D}\sum_{j=1}^{J} d_j n_j\, Sh_j[\rho_{i,s,j} - \rho_{i,\infty} - (\rho_i - \rho_{i,\infty})] \tag{40}$$

using the self-similar representation of the concentration difference in the round brackets and splitting the sum on the right-hand side into two parts, yields for a downstream position z_k on the spray axis the expression

$$S_{i,k} = \underbrace{\pi\mathcal{D}\sum_{j=1}^{J} d_j n_j Sh_j(\rho_{i,s,j} - \rho_{i,\infty})}_{:=B_k} - \Theta(0)\,F(z_k - z_0)^{\beta}\underbrace{\pi\mathcal{D}\sum n_j d_{p,j} Sh_j}_{:=A_k} \tag{41}$$

Equating this formulation with the form eq 26 of the vapor source at $\eta = 0$, where we define the abbreviation $\Lambda := \mathcal{D}_t D^2 \Phi(0)$, yields the equation

$$\underbrace{[\Lambda(z_k - z_0)^{-2\alpha} + \Theta(0)A_k](z_k - z_0)^{\beta}F}_{:=a_k} = B_k \tag{42}$$

so that a minimization of the expression $\sum_k (a_k F - B_k)^2$, i.e., a least-squares fit over all considered axial positions z_k, for a given value of the exponent β, and ambient air relative humidity, yields the corresponding value of the coefficient F. The results obtained for spray 2 from this study are shown in Figure 7.

The correct pairing (β, F) of the exponent and the coefficient is then found by requiring best agreement between the resulting self-similar description of the vapor source and the prediction from the single-droplet evaporation model. The results are listed in Table 2.

The vapor source obtained by this method on the symmetry axes of the three different sprays as given by the self-similar approach (eq 26) and by the single-droplet evaporation model (eq 35) may now be calculated. The results are shown in Figure 8. The agreement achieved is excellent. This close agreement may be attributed to the consistent use of key input data in the single droplet evaporation model. Accordingly, the model is supplied with the self-similar representations of the centerline velocity u_z and vapor concentration ρ_i, obtained from eqs 9 and 25, respectively. Furthermore, the dilute sprays exhibit moderate droplet evaporation rates, leaving the material properties of both phases approximately unchanged. The exponent β is close to a value of 0.1 in all three cases, with slightly higher values in the sprays with the higher Weber numbers. The same is true for the coefficient F, which varies by about a factor of 2 between spray 1 on the one hand and sprays 2 and 3 on the other. The agreement achieved is noteworthy.

The vapor concentration and vapor source fields in the three sprays corresponding to the fits in Figure 8 at the ambient air relative humidity of 30% are shown in Figure 9. The droplet evaporation intensity leads to particularly large vapor concentrations in the shear layer produced by the hollow-cone spray formed by liquid sheet disintegration. Correspondingly, the vapor source has the high values there. The vapor concentration fields in the sprays with the higher values of the exponent β extend wider in the radial direction, indicating the stronger evaporation intensity.

CONCLUSIONS

Based on the self-similar description of the two-phase flow field of pressure-atomized sprays by ref 9, with the gaseous flow field induced by momentum transfer from the liquid phase, the heat and mass transfer from the droplets to the gas phase by evaporation was modeled, and a self-similar description of the transport equation for the concentration of the vapor phase from boundary-layer theory was derived. Possible solutions for the self-similar concentration profiles are presented and discussed. It is found that the vapor source in the spray flow field, which is due to the evaporation of the spray droplets, may be modeled using a single-droplet evaporation model. The model description turns out suitable for representing the self-similar vapor source in the spray flow required for self-similar description of the evaporating spray. Representation of the evaporation behavior of three spray flows studied in our earlier paper Hinterbichler et al.[9] shows that the modeling leads to a compatible self-similar description of both the flow and the vapor concentration fields. For determining the self-similar function in the vapor source, data on the vapor concentration profiles in sprays as investigated is required. With such data available from either experiments or detailed computational simulations, future work will allow the source and related model parameters to be newly determined.

AUTHOR INFORMATION

Corresponding Author

G. Brenn − *Institute of Fluid Mechanics and Heat Transfer, Graz University of Technology, 8010 Graz, Austria;* orcid.org/0000-0001-7576-0790; Phone: +43 (0)316 873 7341; Email: guenter.brenn@tugraz.at; Fax: +43 (0) 316 873 7356

Authors

H. Steiner − *Institute of Fluid Mechanics and Heat Transfer, Graz University of Technology, 8010 Graz, Austria*

H. Hinterbichler − *Institute of Fluid Mechanics and Heat Transfer, Graz University of Technology, 8010 Graz, Austria*

Complete contact information is available at:

https://doi.org/10.1021/acs.iecr.3c01545
Ind. Eng. Chem. Res. 2023, 62, 17041−17051

https://pubs.acs.org/10.1021/acs.iecr.3c01545

Notes

The authors declare no competing financial interest.

■ ACKNOWLEDGMENTS

The authors gratefully acknowledge the financial support from the Austrian Research Promotion Agency FFG (project no. 849876). This work was supported by SIINN ERA-NET, funded under the ERA-NET scheme of the Seventh Framework Programme of the European Commission, Research Directorate - General, Grant Agreement No. 265799.

■ NOMENCLATURE

Latin Symbols

a_t thermal diffusivity (m^2/s)
c_p specific isobaric heat capacity (J/(kg K))
C model constant (m^2/s)
d droplet size (m)
D model constant ($m^{\alpha-1}$)
$\mathcal{D}_t$ effective diffusion coefficient (m^2/s)
E constant (m^2/s)
F model constant ($kg/m^{3+\beta}$)
$f(\eta)$ self-similar shape function
f_d momentum source (m/s^2)
h_{lg} latent enthalpy of evaporation (J/kg)
$\mathcal{H}$ enthalpy flow rate (J/s)
$\mathcal{I}$ momentum flow rate (N)
J number of droplet size classes
$\dot{m}$ mass flow rate (kg/s)
n droplet-number concentration ($1/m^3$)
r radial coordinate (m)
S_i vapor source ($kg/(m^3\ s)$)
$\mathcal{S}_h$ heat source (K/s)
$t(z)$ scaling function (kg/m^3)
T temperature (K)
u_r, u_z velocity components (m/s)
u_0 velocity at the spray axis (m/s)
z axial coordinate (m)
z_0 virtual origin (m)

Abbreviations

PDA phase-doppler anemometry
LIF laser-induced fluorescence

Greek Symbols

α, β model exponents
η self-similar coordinate
$\Theta(\eta)$ self-similar vapor concentration
μ dynamic viscosity (Pa s)
ν, ν_t kinematic and eddy viscosity (m^2/s)
ρ density, concentration (kg/m^3)
σ surface tension (N/m)
$\Phi(\eta)$ self-similar vapor source
Ψ Stokesian stream function (m^3/s)
$\Omega(\eta)$ self-similar momentum source

Subscripts

i vapor component
j droplet size class
l liquid phase
or property at the atomizer orifice
r radial direction
s droplet surface
t turbulent
z axial direction
∞ far field

Nondimensional Groups

Le Lewis number
Oh Ohnesorge number
Pr Prandtl number
Re Reynolds number
Sc Schmidt number
We Weber number

■ REFERENCES

(1) Lefebvre, A. H.; McDonell, V. G. *Atomization and Sprays*, 2nd ed.; Taylor & Francis, CRC Press: Boca Raton, FL, 2017.
(2) Ashgriz, N., Ed. *Handbook of Atomization and Sprays*; Springer: New York, 2011.
(3) Kessler, R. Engineered nanoparticles in consumer products: Understanding a new ingredient. *Environ. Health Perspect.* **2011**, *119*, A120−A125.
(4) Brenn, G. *Analytical Solutions for Transport Processes*; Springer: Berlin, Heidelberg, 2017.
(5) Schlichting, H. Laminare Strahlausbreitung. *Z. Angew. Math. Mech.* **1933**, *13*, 260−263.
(6) Wygnanski, I.; Fiedler, H. Some measurements in the self-preserving jet. *J. Fluid Mech.* **1969**, *38*, 577−612.
(7) Hussein, H. J.; Capp, S. P.; George, W. K. Velocity measurements in a high-Reynolds-number, momentum-conserving, axisymmetric, turbulent jet. *J. Fluid Mech.* **1994**, *258*, 31−75.
(8) Wu, K.-J.; Santavicca, D. A.; Bracco, F. V.; Coghe, A. LDV measurements of drop velocity in diesel-type sprays. *AIAA J.* **1984**, *22*, 1263−1270.
(9) Hinterbichler, H.; Steiner, H.; Brenn, G. Self-similar pressure-atomized sprays. *J. Fluid Mech.* **2020**, *889*, A17.
(10) Soltani, M. R.; Ghorbanian, K.; Ashjaee, M.; Morad, M. R. Spray characteristics of a liquid−liquid coaxial swirl atomizer at different mass flow rates. *Aerosp. Sci. Technol.* **2005**, *9*, 592−604.
(11) Cossali, G. E. An integral model for gas entrainment into full cone sprays. *J. Fluid Mech.* **2001**, *439*, 353−366.
(12) Dhivyaraja, K.; Gaddes, D.; Freeman, E.; Tadigadapa, S.; Panchagnula, M. V. Dynamical similarity and universality of drop size and velocity spectra in sprays. *J. Fluid Mech.* **2019**, *860*, 510−543.
(13) Li, X.; Shen, J. Experimental Study of Sprays from Annular Liquid Jet Breakup. *J. Propuls. Power* **1999**, *15*, 103−110.
(14) Ariyapadi, S.; Balachandar, R.; Berruti, F. Spray characteristics of two-phase feed nozzles. *Can. J. Chem. Eng.* **2003**, *81*, 923−939.
(15) Panchagnula, M. V.; Sojka, P. E. Spatial droplet velocity and size profiles in effervescent atomizer-produced sprays. *Fuel* **1999**, *78*, 729−741.
(16) George, W. K. In *Advances in Turbulence*; George, W. K., Arndt, R., Eds.; Hemisphere: New York, 1989; pp 39−73.
(17) Karpetis, A. N.; Gomez, A. Self-similarity, momentum scaling and Reynolds stress in non-premixed turbulent spray flames. *J. Fluid Mech.* **1999**, *397*, 231−258.
(18) Russo, S.; Gomez, A. Physical characterization of laminar spray flames in the pressure range 0.1−0.9 MPa. *Combust. Flame* **2006**, *145*, 339−356.
(19) Kourmatzis, A.; Pham, P. X.; Masri, A. R. Characterization of atomization and combustion in moderately dense turbulent spray flames. *Combust. Flame* **2015**, *162*, 978−996.
(20) Shearer, A. J.; Tamura, H.; Faeth, G. M. Evaluation of a locally homogeneous flow model of spray evaporation. *J. Energy* **1979**, *3*, 271−278.
(21) Faeth, G. M. Evaporation and combustion of sprays. *Prog. Energy Combust. Sci.* **1983**, *9*, 1−76.
(22) Petranović, Z.; Edelbauer, W.; Vujanović, M.; Duić, N. Modelling of spray and combustion processes by using the Eulerian multiphase approach and detailed chemical kinetics. *Fuel* **2017**, *191*, 25−35.

(23) Barenblatt, G I; Zel'dovich, Y B Self-similar solutions as intermediated asymptotics. *Annu. Rev. Fluid Mech.* **1972**, *4*, 285−312.
(24) Tropea, C.; Yarin, A.; Foss, J. F. *Springer Handbook of Experimental Fluid Mechanics*; Springer-Verlag: Berlin Heidelberg, 2007.
(25) Tominaga, Y.; Stathopoulos, T. Turbulent Schmidt numbers for CFD analysis with various types of flowfield. *Atmos. Environ.* **2007**, *41*, 8091−8099.
(26) Frössling, N. Über die Verdunstung fallender Tropfen. *Gerlands Beitr. Geophys.* **1938**, *52*, 170−216.
(27) Abramzon, A.; Sirignano, W. Drop vaporisation model for spray combustion calculations. *Int. J. Heat Mass Transfer* **1989**, *32*, 1605−1618.
(28) Smolander, S. *Lecture Notes on Thermodynamics*; University of Helsinki, 2015.
(29) Hyland, R. W.; Wexler, A. Formulations for the thermodynamic properties of saturated phases of H2O. *ASHRAE Trans.* **1983**, *89*, 500−511.

https://doi.org/10.1021/acs.iecr.3c01545
Ind. Eng. Chem. Res. 2023, 62, 17041−17051